

Naphthalene diimide-based small molecular acceptors for organic solar cells

Kira Rundel,^a Subashani Maniam,^b Kedar Deshmukh,^a Eliot Gann,^{a,c} Shyamal K. K. Prasad,^d Justin M. Hodgkiss,^d Steven Langford,^b and Christopher R. McNeill^a

^a Department of Materials Science and Engineering, Monash University, Wellington Road, Clayton, VIC 3800, Australia

^b School of Chemistry, Monash University, Wellington Road, Clayton, VIC 3800, Australia

^c Australian Synchrotron, 800 Blackburn Road, Clayton, VIC 3168, Australia

^d MacDiarmid Institute for Advanced Materials and Nanotechnology, Victoria University of Wellington, Wellington 6140, New Zealand

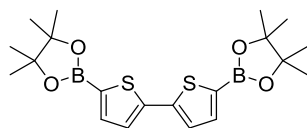
Electronic Supporting Information

Content

1. Additional Synthesis	2
2. NMR Spectra	5
3. Cyclic Voltammetry	14
4. Absorbance	16
5. Device Optimization	18
6. 1D GIWAXS Line Cut Profiles	21
7. Photoluminescence Quenching	22

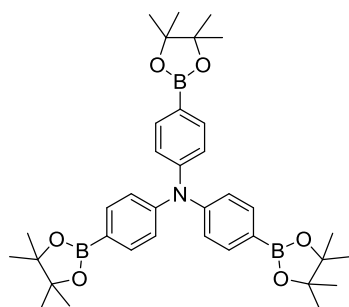
1. Additional Synthesis

5,5'-bis(4,4,5,5-tetramethyl-1,3,2-dioxaborolan-2-yl)-2,2'-bithiophene



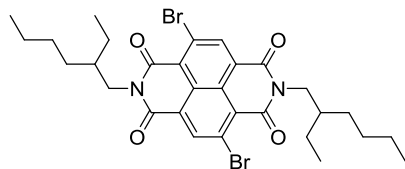
Off white solid (2.85 g, 56%). M.p. 210-211 °C. ¹H NMR (400 MHz, CDCl₃) δ 7.52 (d, *J* = 3.6, 2H, ArH), 7.28 (d, *J* = 3.6, 2H, ArH), 1.35 (s, 24H, CH₃). ¹³C NMR (100 MHz, CDCl₃) δ 144.0, 138.1, 125.8, 84.4, 24.9. LRMS (ESI) *m/z* obsd [M+Na]⁺ 441.1, calcd C₂₀H₂₈B₂NaO₄S₂ [M+Na]⁺ 441.2.

tris(4-(4,4,5,5-tetramethyl-1,3,2-dioxaborolan-2-yl)phenyl)amine



White solid (4.20 g, 83%). M.p. >300 °C. ¹H NMR (400 MHz, CDCl₃) δ 7.69-7.67 (m, 6H, ArH), 7.09-7.06 (m, 6H, ArH), 1.34 (s, 36H, CH₃). ¹³C NMR (100 MHz, CDCl₃) δ 149.9, 136.1, 123.6, 83.8, 25.0. LRMS (ESI) *m/z* obsd [M+Na]⁺ 646.3, calcd C₃₆H₄₈B₃NNaO₆ [M+Na]⁺ 646.2.

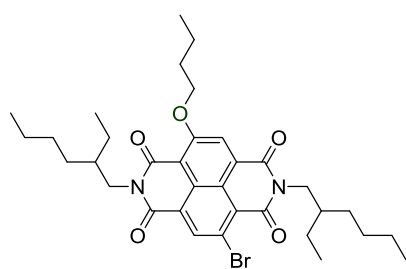
4,9-dibromo-2,7-bis(2-ethylhexyl)benzo[*lmn*][3,8]phenanthroline-1,3,6,8(2*H*,7*H*)-tetraone



Yellow solid (600 mg, 30%). M.p. 246-248 °C. ¹H NMR (400 MHz, CDCl₃) δ 9.00 (s, 2H, NDI), 4.20-4.11 (m, 4H, CH₂), 1.97-1.91 (m, 2H, CH), 1.41-1.25 (m, 16H, CH₂), 0.95-0.87 (m, 12, CH₃). ¹³C NMR (100 MHz, CDCl₃) δ 161.4, 161.2, 139.3, 128.5, 127.9, 125.5, 124.3, 45.3, 37.9, 30.8, 28.7, 24.1, 23.2, 14.2, 10.7. LRMS (ESI) *m/z* obsd [M+H]⁺ 649.1, calcd C₃₀H₃₇Br₂N₂O₄ [M+H]⁺ 649.1.

4-bromo-9-butoxy-2,7-bis(2-ethylhexyl)benzo[*lmn*][3,8]phenanthroline-1,3,6,8(2*H*,7*H*)-tetraone (Compound 1)

4,9-dibromo-2,7-bis(2-ethylhexyl)benzo[*lmn*][3,8]phenanthroline-1,3,6,8(2*H*,7*H*)-tetraone

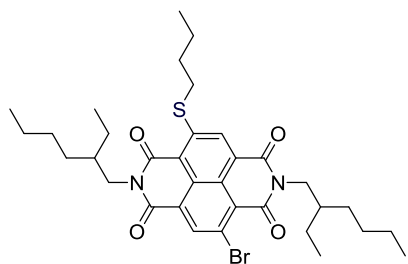


(0.20 g, 0.31 mmol) was dissolved in chloroform (40 mL). Then, K₂CO₃ (0.43 g, 3.1 mmol) and butyl alcohol (0.11 mL, 1.2 mmol) were added to the solution and heated under reflux for 24 h. Dichloromethane (30 mL) was added to the reaction mixture and the solution was washed with water (3 × 30 mL). The organic phase was collected, dried over anhydrous MgSO₄ and the solvent removed under vacuum. The crude product was purified by column chromatography with using 30% *n*-hexane in dichloromethane to give title compound as a bright yellow solid (150 mg, yield 76%). M.p. 131-132 °C. ¹H NMR (400 MHz, CDCl₃) δ 8.93 (s, 1H, NDI), 8.51 (s, 1H, NDI), 4.49 (t, *J* = 6.8, 2H, OCH₂), 4.20-4.07 (m, 4H, NCH₂), 2.05-1.91 (m, 4H, CH &

CH₂), 1.69-1.58 (m, 2H, CH₂), 1.41-1.27 (m, 16H, CH₂), 1.04 (t, *J* = 7.6, 3H, CH₃), 0.96-0.92 (m, 12H, CH₃). ¹³C NMR (100 MHz, CDCl₃) δ 162.3, 162.2, 162.0, 161.6, 161.1, 139.1, 128.5, 127.6, 125.5, 125.1, 123.6, 123.5, 120.0, 111.3, 70.8, 45.2, 44.5, 38.0, 37.8, 30.83, 30.78, 28.73, 28.71, 24.2, 24.1, 23.2, 19.2, 14.2, 13.9, 10.8, 10.7. HRMS (ESI) *m/z* obsd [M+H]⁺ 641.2590, calcd C₃₄H₄₆BrN₂O₅ [M+H]⁺ 641.2585.

4-bromo-9-(butylthio)-2,7-bis(2-ethylhexyl)benzo[lmn][3,8]phenanthroline-1,3,6,8(2H,7H)-tetraone (Compound 2)

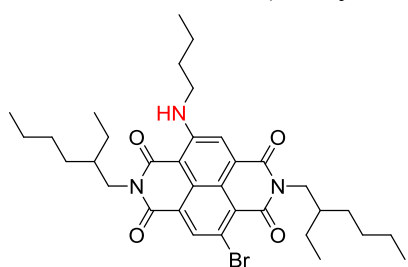
4,9-dibromo-2,7-bis(2-ethylhexyl)benzo[lmn][3,8]phenanthroline-1,3,6,8(2H,7H)-tetraone (0.20 g, 0.31 mmol) was dissolved in chloroform (40 mL). Then, K₂CO₃ (0.43 g, 3.1 mmol) and butyl thiol (0.13 mL, 1.2 mmol) were added to the solution and heated at 50 °C for 24 h. Dichloromethane (30 mL) was added to the reaction mixture and the solution was washed with water (3 × 30 mL). The organic phase was collected, dried over anhydrous MgSO₄ and the solvent removed under vacuum. The crude product was purified by column chromatography with using



30% *n*-hexane in dichloromethane to give title compound as a deep orange solid (100 mg, yield 49%). M.p. 145-146 °C. ¹H NMR (400 MHz, CDCl₃) δ 8.96 (s, 1H, NDI), 8.77 (s, 1H, NDI), 4.21-4.11 (m, 4H, NCH₂), 3.23 (t, *J* = 7.6, 2H, SCH₂), 2.00-1.83 (m, 4H, CH & CH₂), 1.68-1.58 (m, 2H, CH₂), 1.42-1.29 (m, 16H, CH₂), 1.03 (t, *J* = 7.6, 3H, CH₃), 0.96-0.86 (m, 12H, CH₃). ¹³C NMR (100 MHz, CDCl₃) δ 163.7, 162.6, 161.9, 161.6, 151.7, 138.9, 129.1, 127.5, 125.8, 125.6, 124.7, 124.5, 123.8, 119.4, 45.3, 45.0, 38.0, 37.9, 32.3, 30.81, 30.75, 30.0, 29.9, 28.71, 28.69, 24.2, 24.1, 23.2, 22.5, 14.3, 14.2, 13.9, 10.8, 10.7. HRMS (ESI) *m/z* obsd [M+H]⁺ 657.2360, calcd C₃₄H₄₆BrN₂O₄S [M+H]⁺ 657.2356.

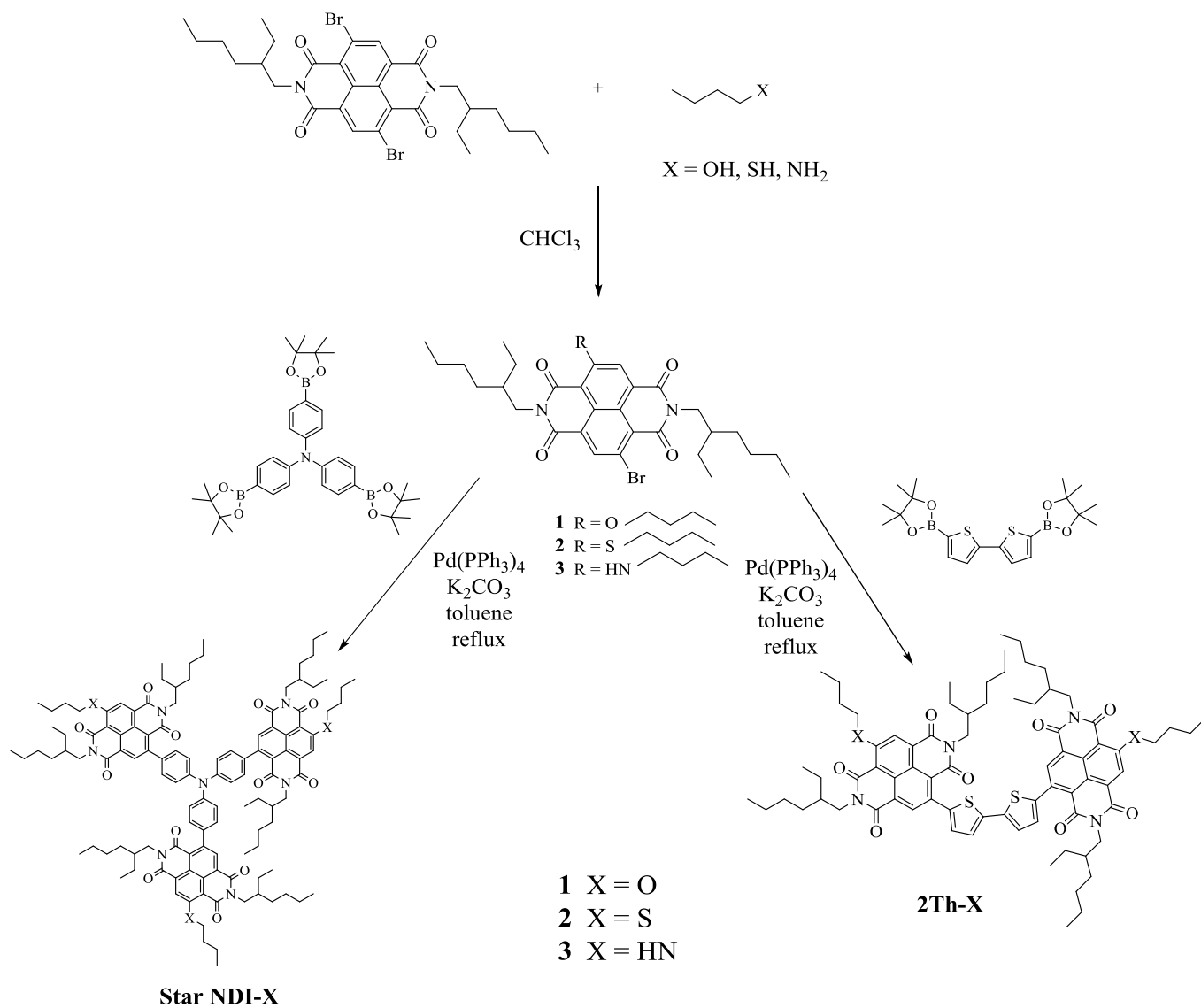
4-bromo-9-(butylamino)-2,7-bis(2-ethylhexyl)benzo[lmn][3,8]phenanthroline-1,3,6,8(2H,7H)-tetraone (Compound 3)

4,9-dibromo-2,7-bis(2-ethylhexyl)benzo[lmn][3,8]phenanthroline-1,3,6,8(2H,7H)-tetraone (50 mg, 77.1 μmol) was dissolved in chloroform (40 mL). Butyl amine (4 mL, excess) were added to the solution stirred at room temperature. Dichloromethane (30 mL) was added to the reaction mixture and the solution was washed with water (3 × 30 mL). The organic phase was collected, dried over anhydrous MgSO₄ and the solvent removed under vacuum. The crude product was purified by column chromatography with using dichloromethane to give title



compound as a deep blue solid (45 mg, yield 91%). M.p. 246-248 °C. ¹H NMR (400 MHz, CDCl₃) δ 10.09 (t, *J* = 5.6, 1H, NH), 8.85 (s, 1H, NDI), 8.27 (s, 1H, NDI), 4.18-4.06 (m, 4H, NCH₂), 3.61-3.56 (m, 2H, HNCH₂), 1.95-1.89 (m, 2H, CH), 1.86-1.78 (m, 2H, CH₂), 1.59-1.50 (m, 2H, CH₂), 1.39-1.29 (m, 16H, CH₂), 1.03 (t, *J* = 7.6, 3H, CH₃), 0.95-0.86 (m, 12H, CH₃). ¹³C NMR (100 MHz, CDCl₃) δ 166.5, 162.7, 162.4, 161.9, 152.0, 138.5, 128.9, 127.5, 123.6, 123.5, 121.6, 120.8, 120.4, 100.7, 45.1, 44.3, 43.2, 38.0, 37.9, 31.6, 30.8, 28.8, 24.2, 23.2, 20.4, 14.2, 13.9, 10.81, 10.76. HRMS (ESI) *m/z* obsd [M+H]⁺ 640.2748, calcd C₃₄H₄₇BrN₃O₄ [M+H]⁺ 640.2744.

Figure ES1. Reaction scheme for the molecular acceptors.



2. NMR Spectra

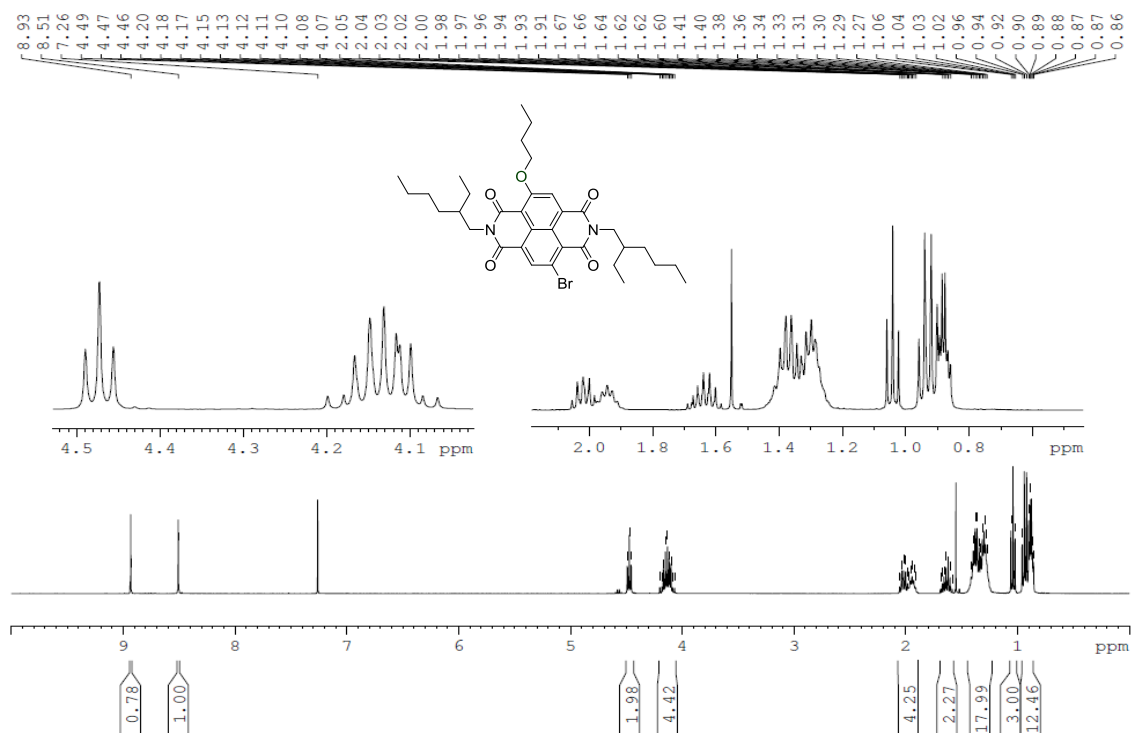


Figure ES2. 400 MHz ^1H NMR (300 K, CDCl_3) spectrum of compound **1**.

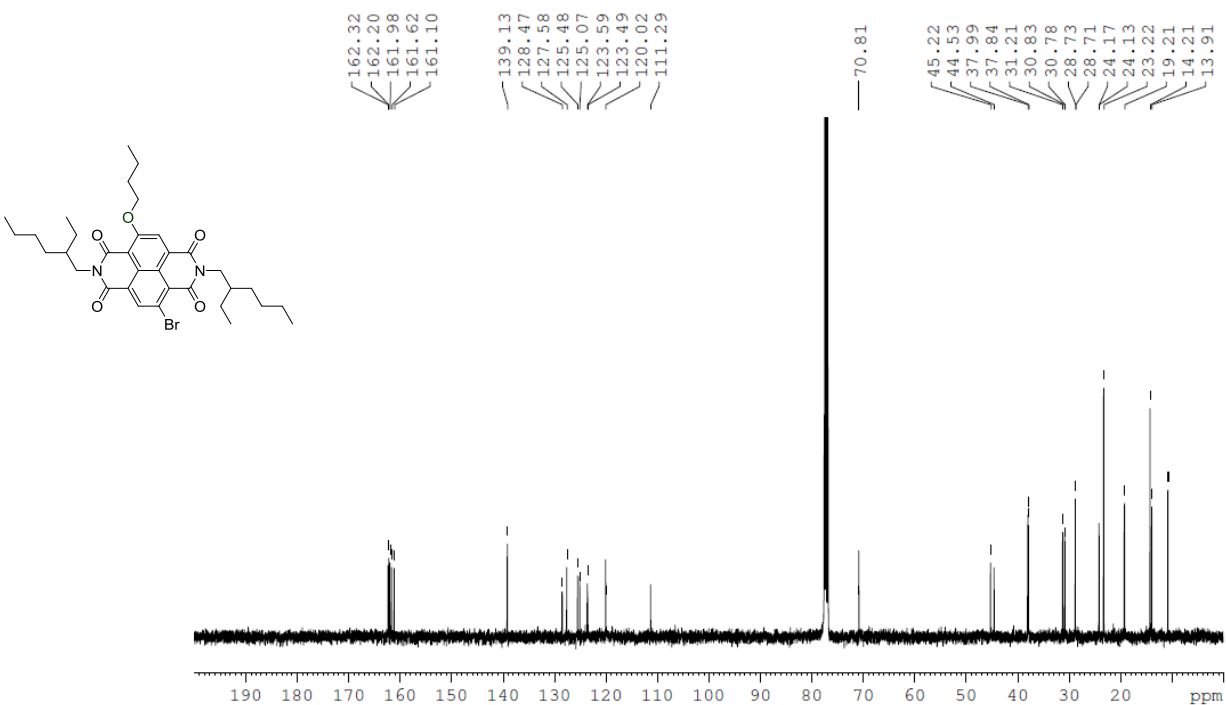


Figure ES3. 100 MHz ^{13}C NMR (300 K, CDCl_3) spectrum of compound **1**.

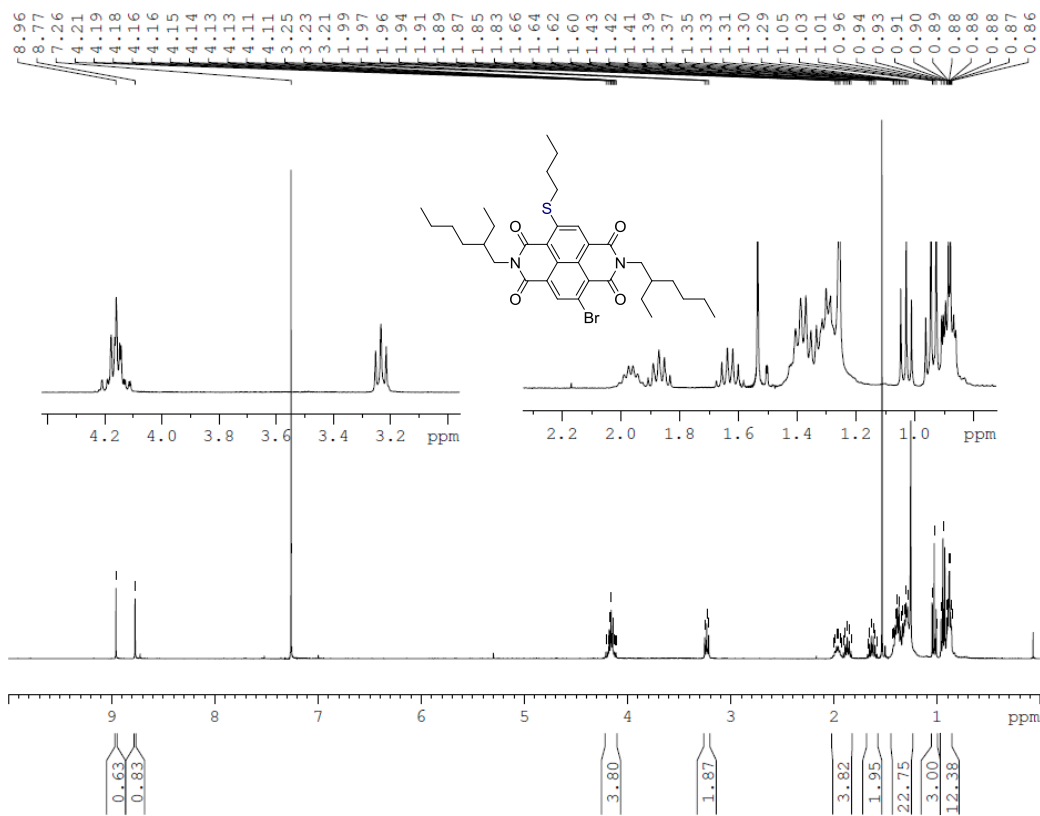


Figure ES4. 400 MHz ¹H NMR (300 K, CDCl₃) spectrum of compound 2.

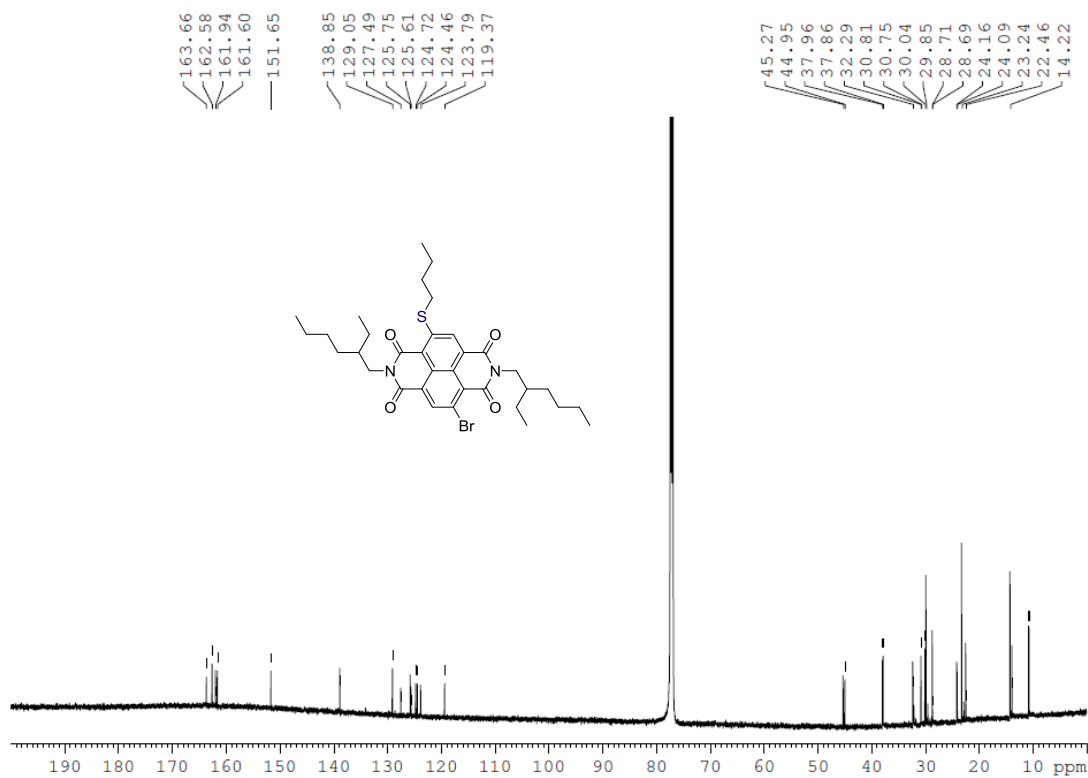


Figure ES5. 100 MHz ¹³C NMR (300 K, CDCl₃) spectrum of compound 2.

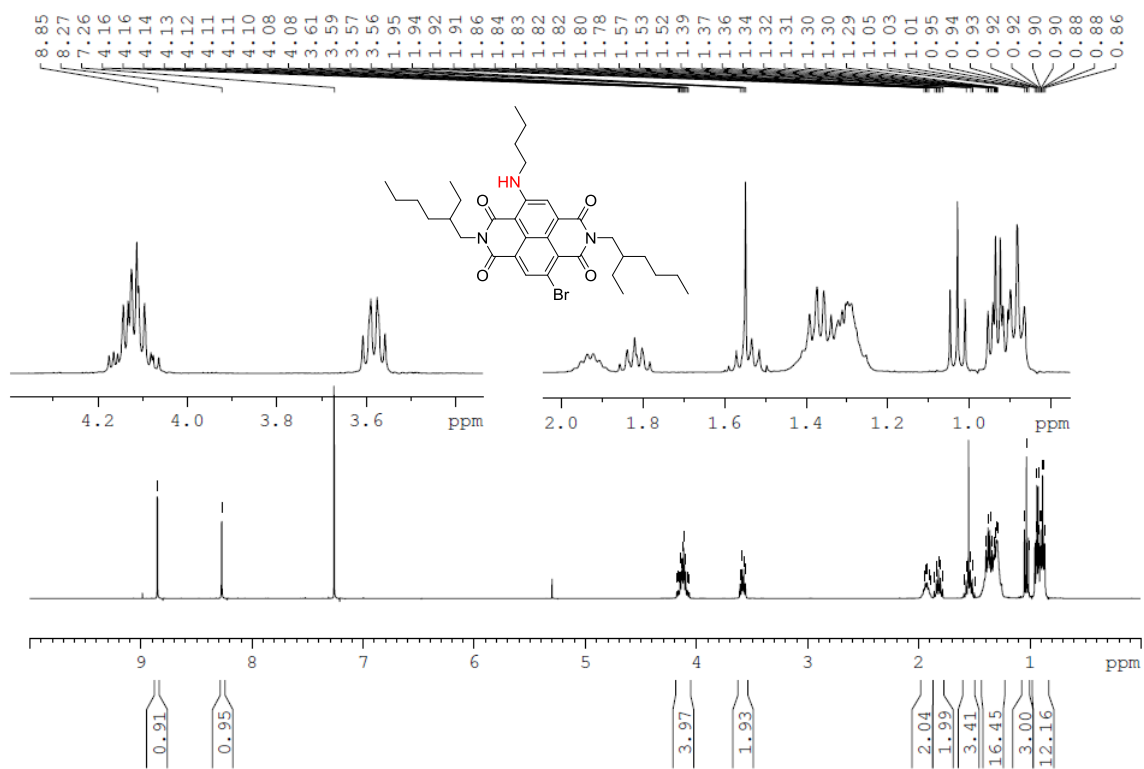


Figure ES6. 400 MHz ^1H NMR (300 K, CDCl_3) spectrum of compound 3.

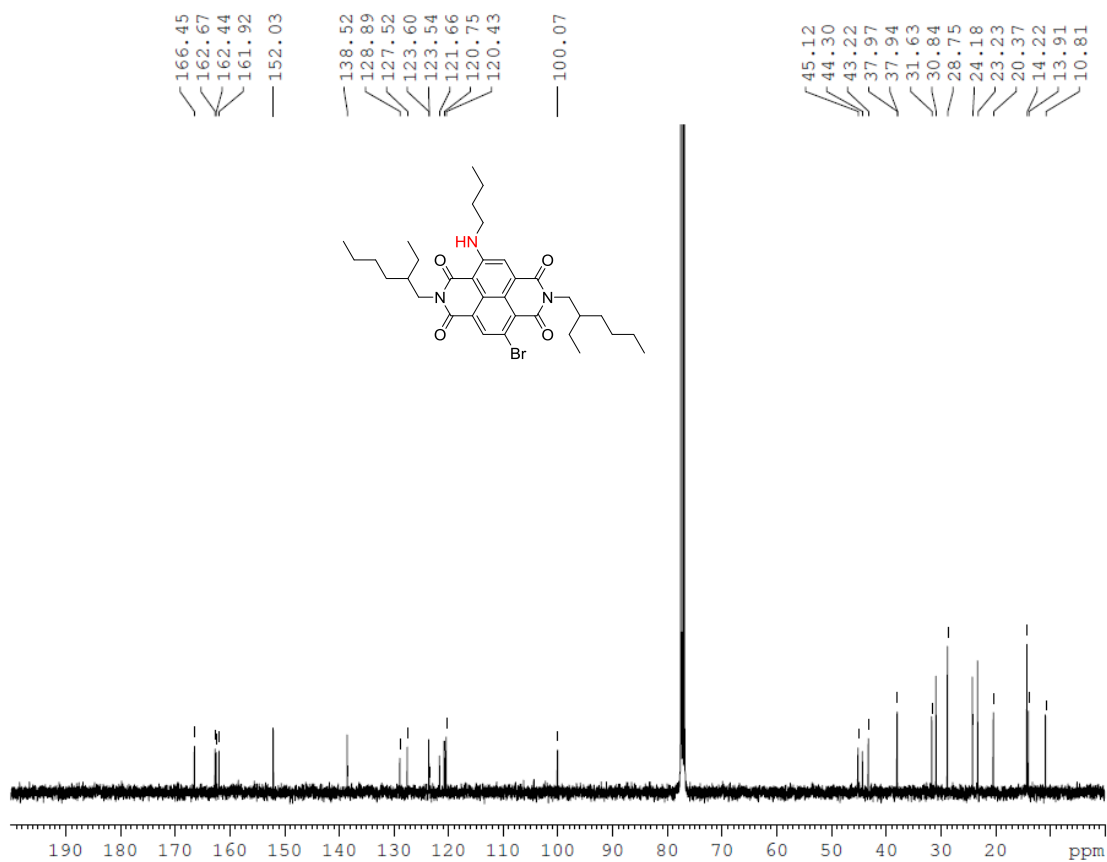


Figure ES7. 100 MHz ^{13}C NMR (300 K, CDCl_3) spectrum of compound 3.

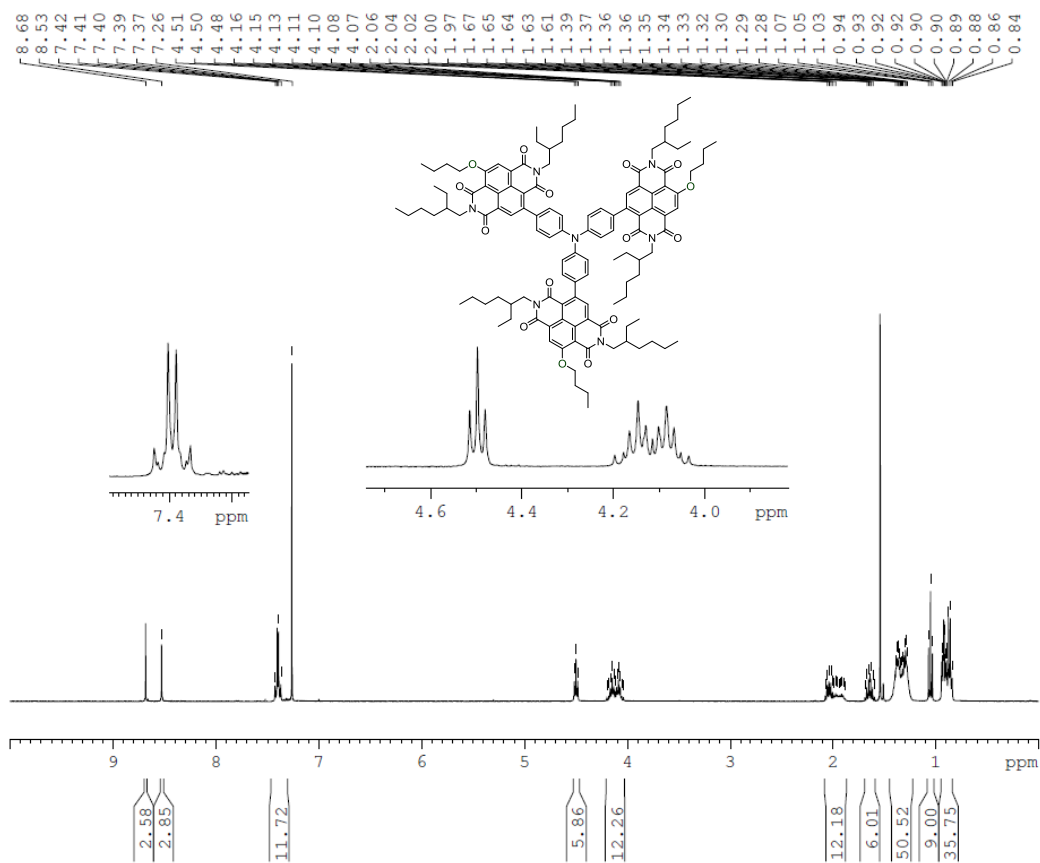


Figure ES8. 400 MHz ^1H NMR (300 K, CDCl_3) spectrum of compound *Star NDI-O*.

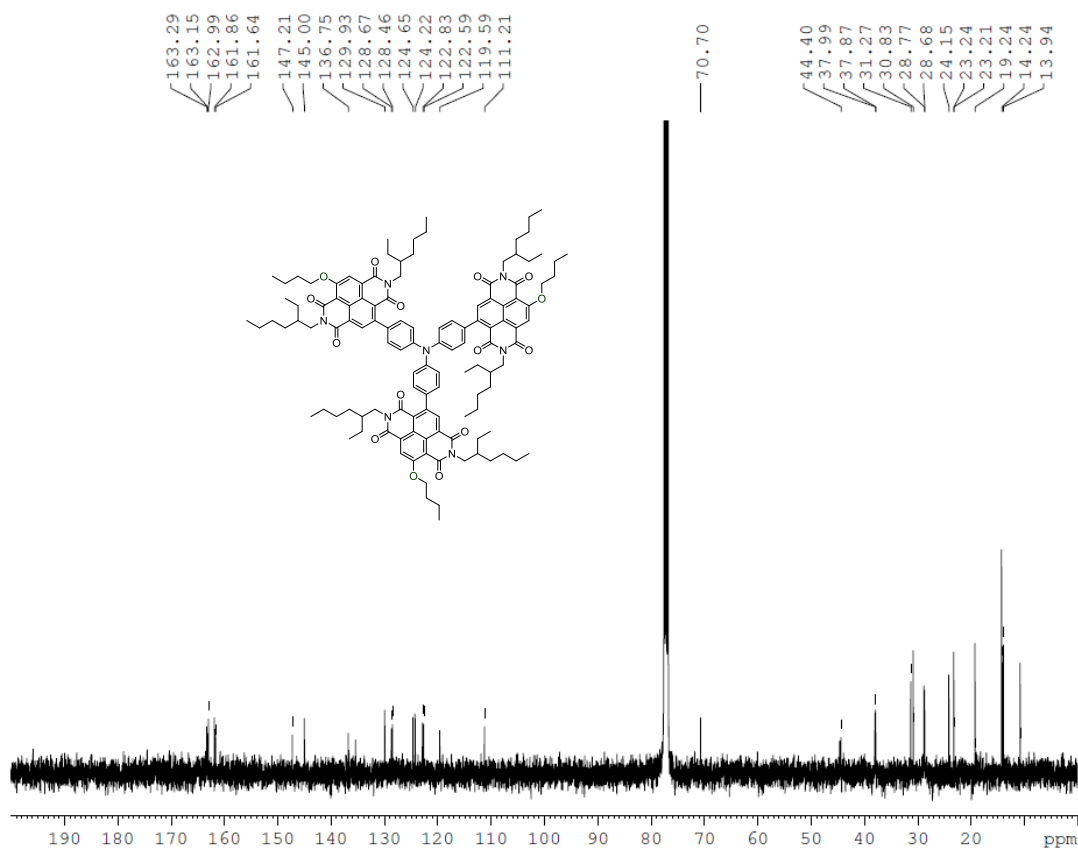


Figure ES9. 100 MHz ^{13}C NMR (300 K, CDCl_3) spectrum of compound *Star NDI-O*.

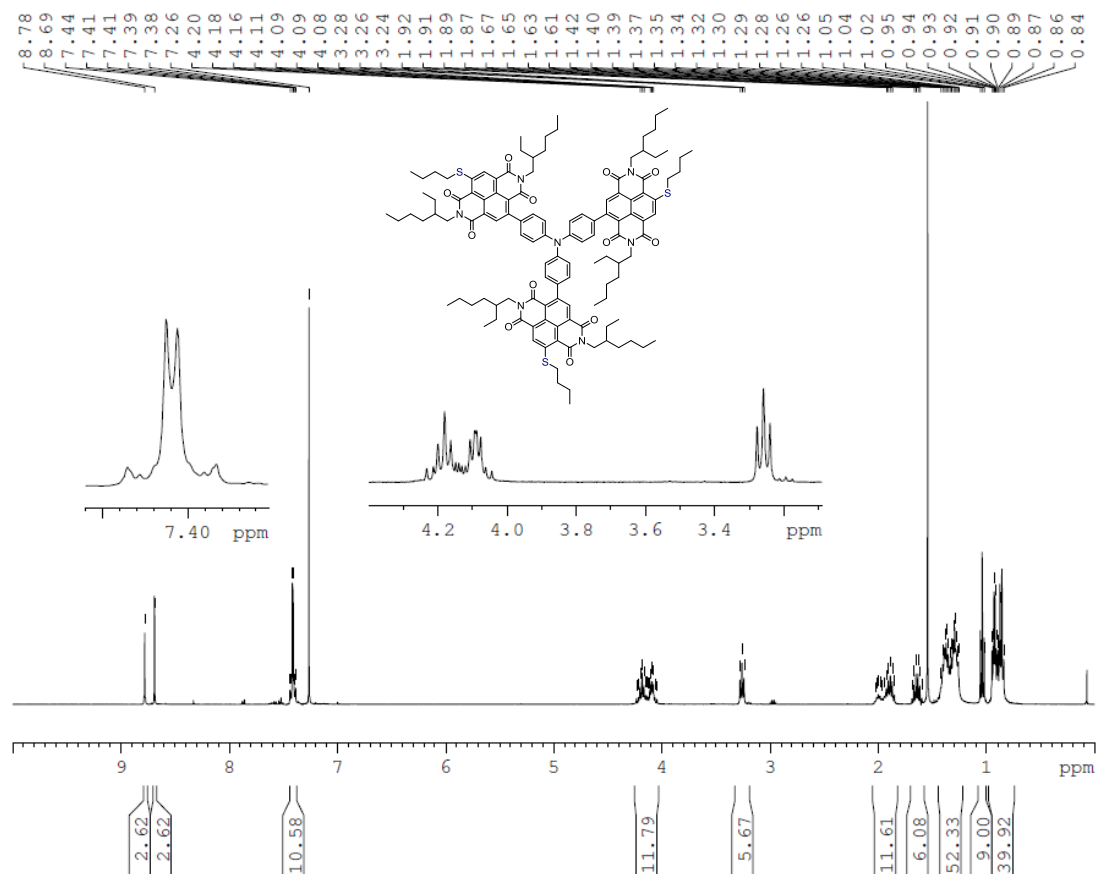


Figure ES10. 400 MHz ^1H NMR (300 K, CDCl_3) spectrum of compound *Star NDI-S*.

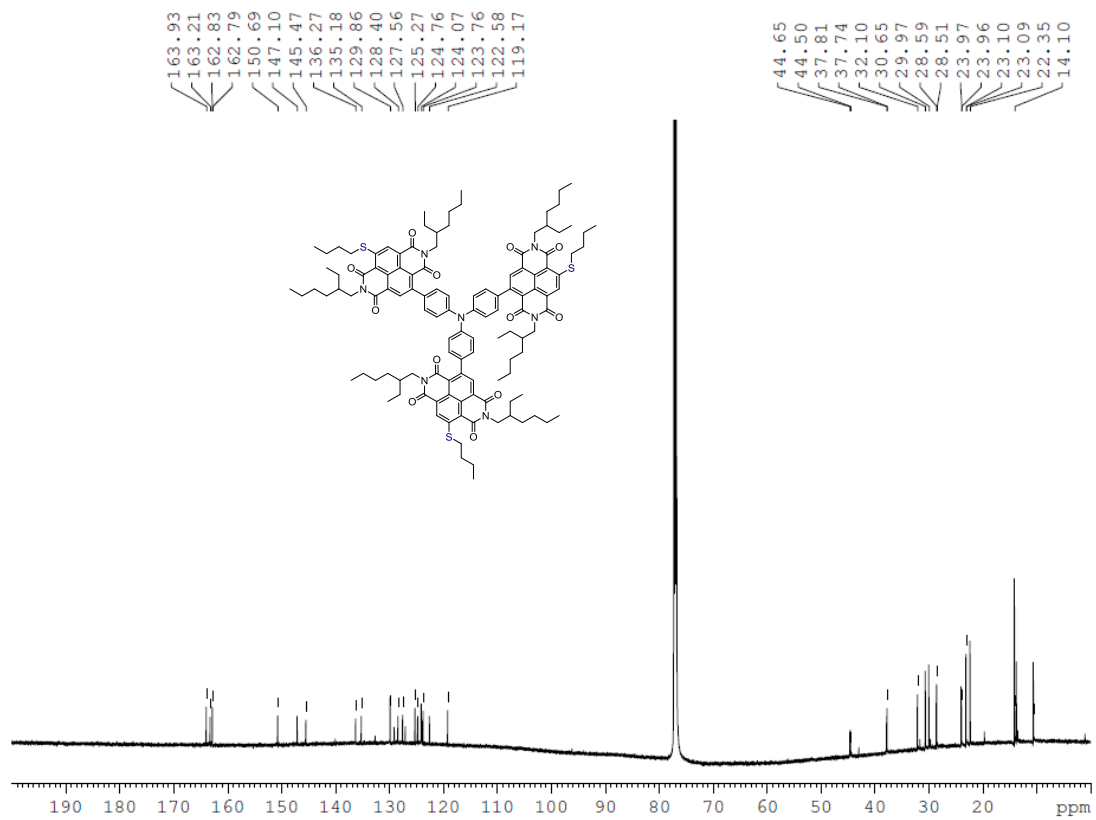


Figure ES11. 150 MHz ^{13}C NMR (300 K, CDCl_3) spectrum of compound *Star NDI-S*.

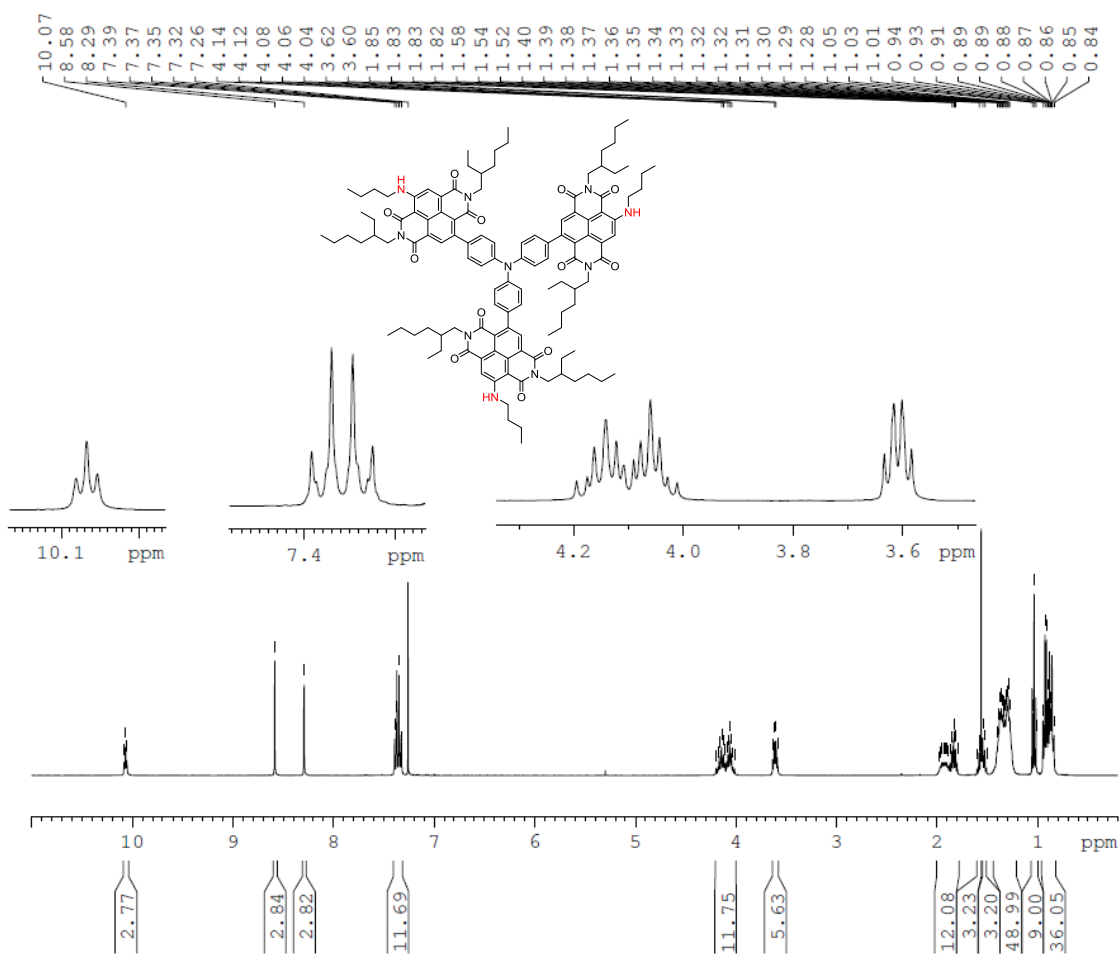


Figure ES12. 400 MHz ¹H NMR (300 K, CDCl₃) spectrum of compound *Star NDI-N*.

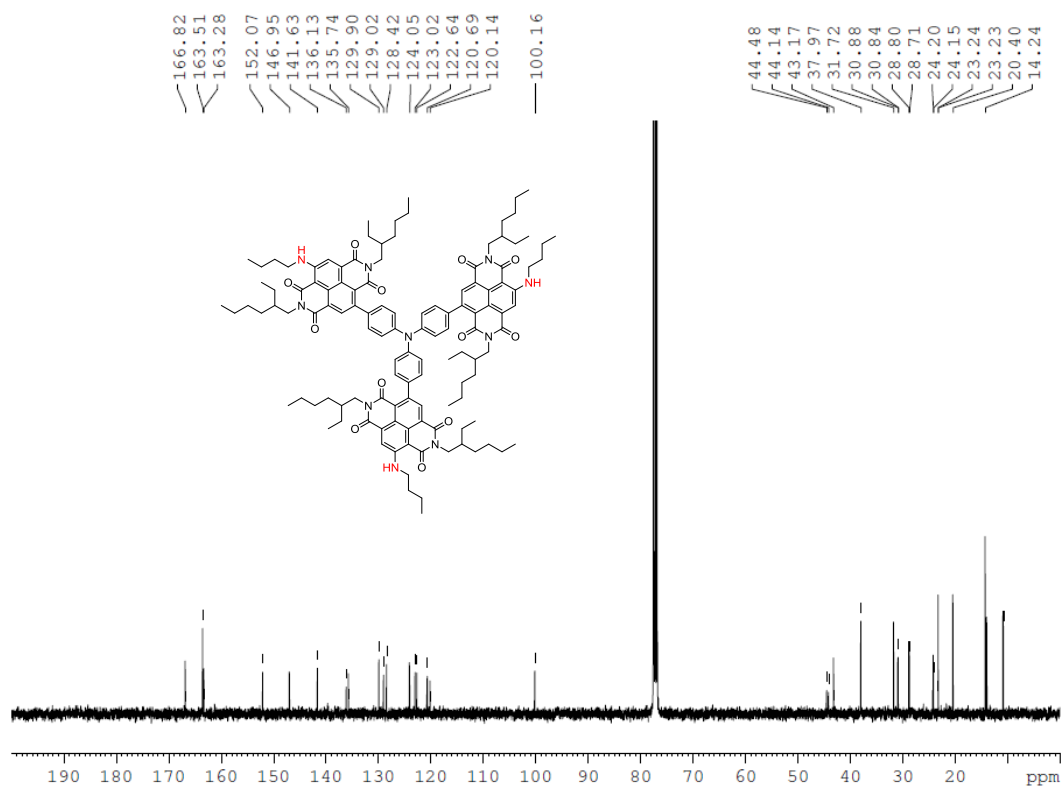


Figure ES13. 100 MHz ¹³C NMR (300 K, CDCl₃) spectrum of compound *Star NDI-N*.

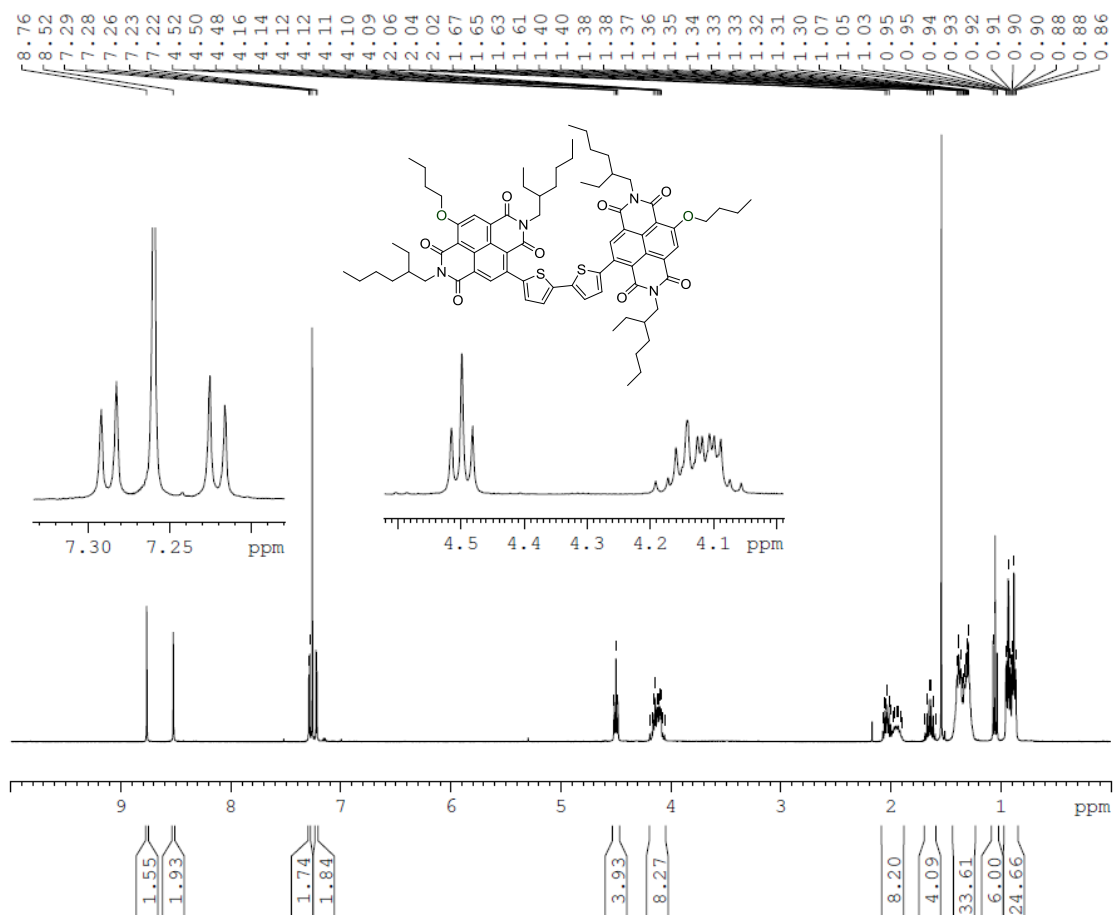


Figure ES14. 400 MHz ^1H NMR (300 K, CDCl_3) spectrum of compound **2Th-O**.

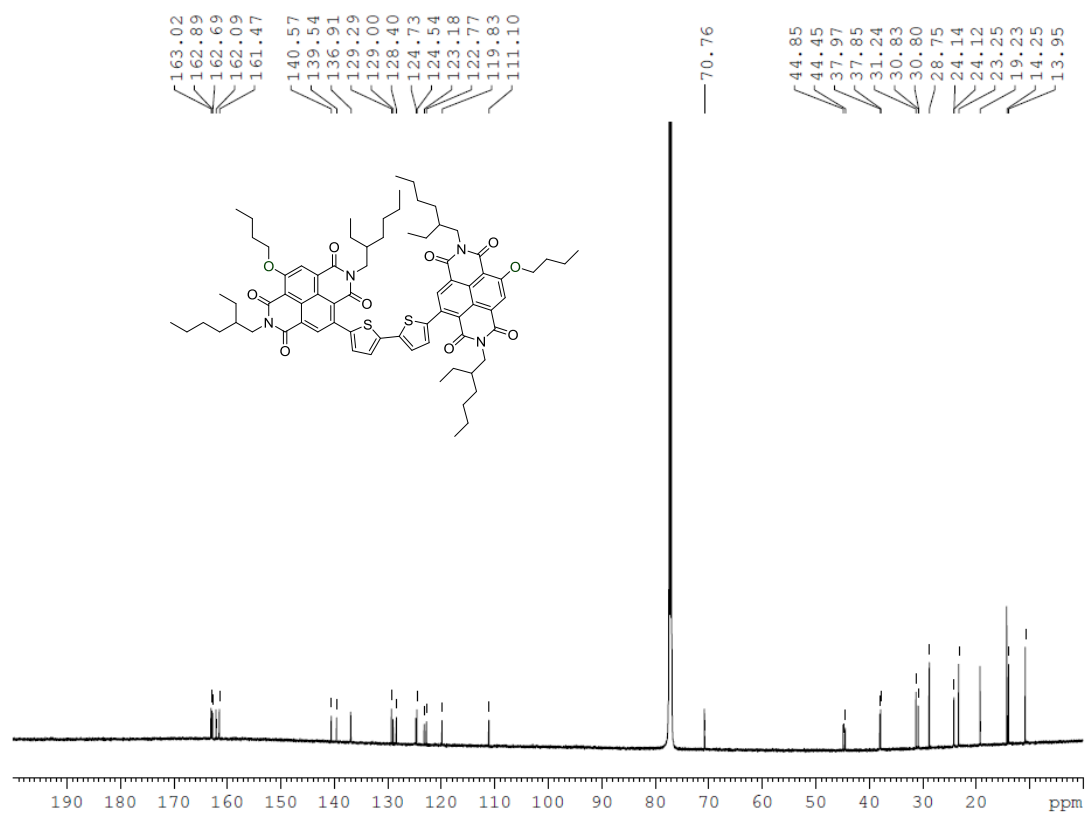


Figure ES15. 150 MHz ^{13}C NMR (300 K, CDCl_3) spectrum of compound **2Th-O**.

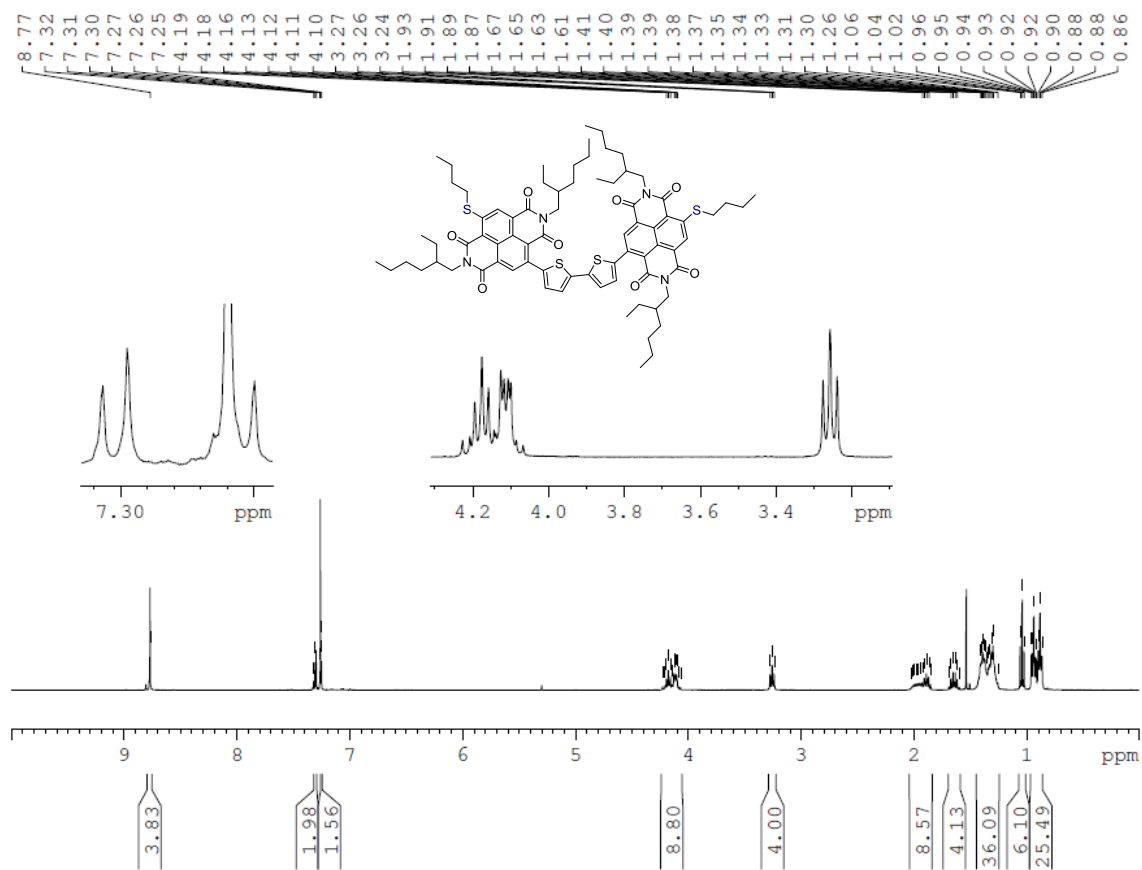


Figure ES16. 400 MHz ^1H NMR (300 K, CDCl_3) spectrum of compound **2Th-S**.

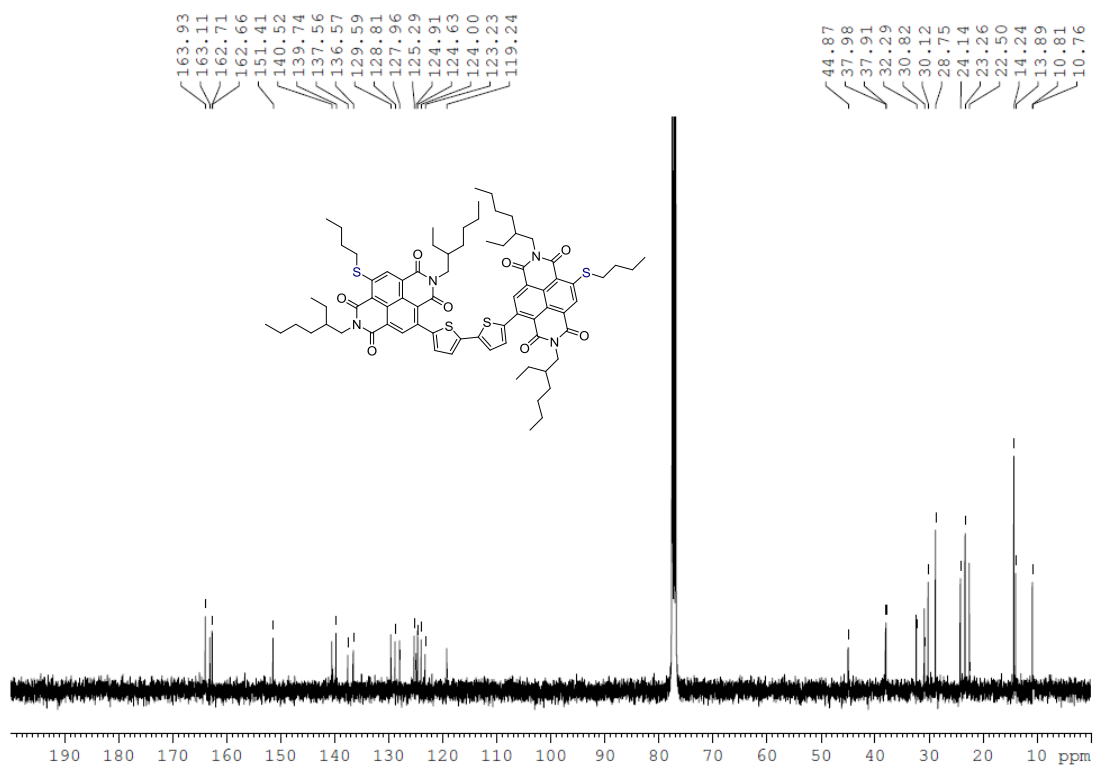


Figure ES17. 150 MHz ^{13}C NMR (300 K, CDCl_3) spectrum of compound **2Th-S**.

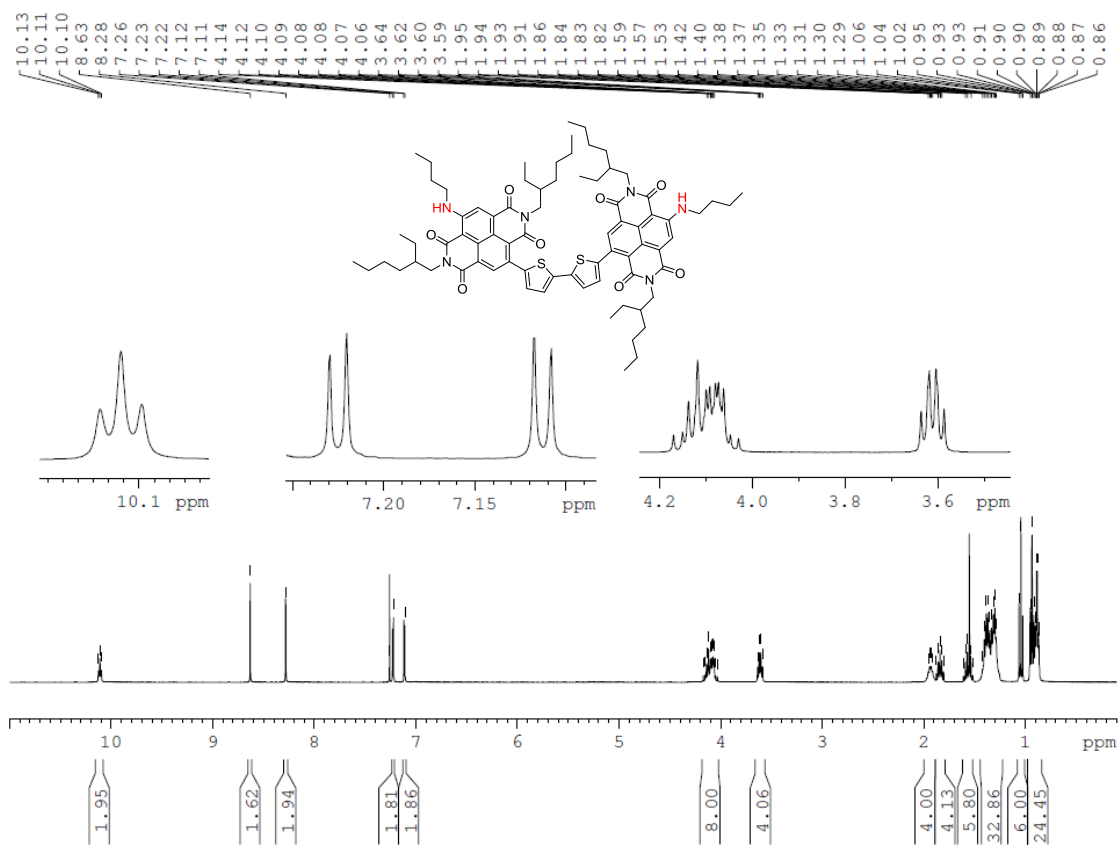


Figure ES18. 400 MHz ¹H NMR (300 K, CDCl₃) spectrum of compound **2Th-N**.

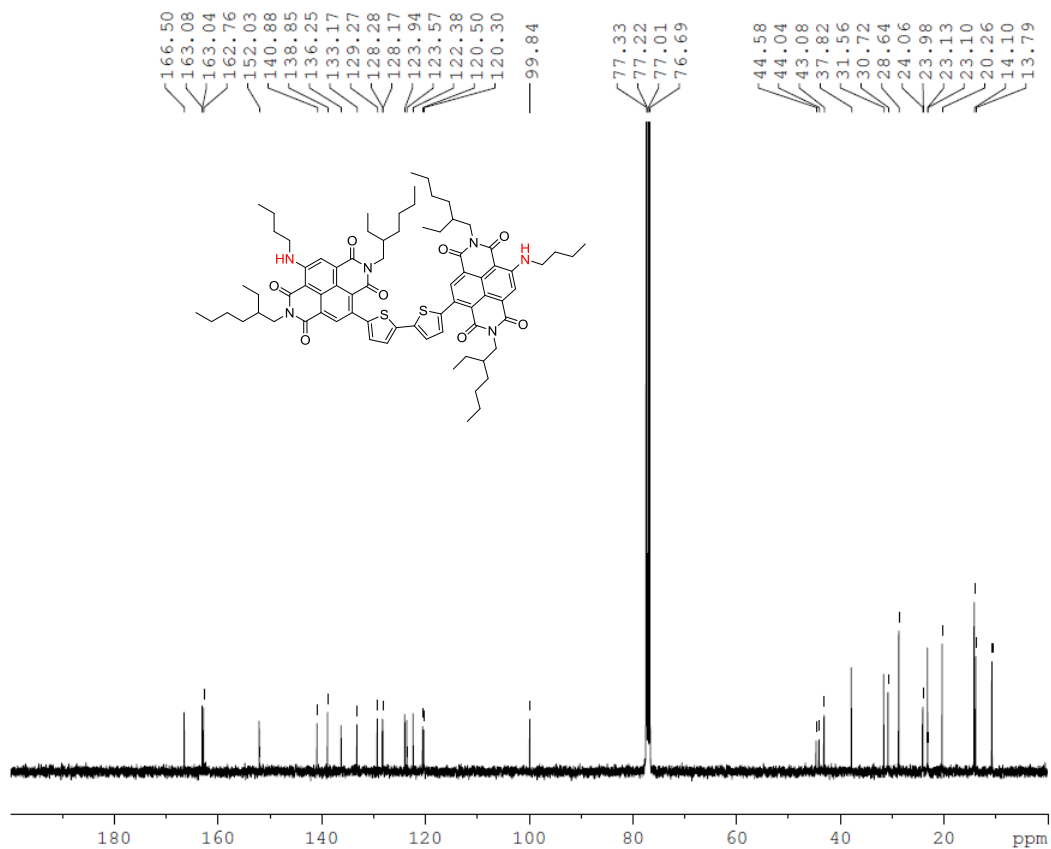


Figure ES19. 100 MHz ¹³C NMR (300 K, CDCl₃) spectrum of compound **2Th-N**.

3. Cyclic Voltammetry

A Powerlab ML160 potentiostat interfaced via a Powerlab 4/20 controller to a PC running Echem for Windows was used for the solution-based cyclic voltammetry measurements. Argon-purified dichloromethane was used as the solvent for tetrabutylammonium hexafluorophosphate (Bu_4NPF_6) (0.1 M), the supporting electrolyte. 0.05M of each acceptor material was then added to this solution prior to measurements. All CV measurements were made at room temperature using a glassy carbon working electrode (2.0 mm diameter), a platinum wire counter electrode and a second platinum wire as a quasi-reference electrode, separated from the bulk of the solution by a frit. This system was internally calibrated with ferrocene/ferrocenium (Fc/Fc^+). A scan rate of 100 mV/s was used for all measurements, with voltammograms recorded within a range from -2000 to 1500 mV. LUMO values were extracted from the first reduction peak using the following equations, assuming the Fc/Fc^+ redox reaction takes place at 4.8 eV with respect to vacuum:

$$E_{1/2} = \frac{E_{p1,\text{red}} + E_{p1,\text{ox}}}{2} - E_{1/2 \text{ Fc}/\text{Fc}^+}$$

$$E_{\text{LUMO}} = -(E_{1/2} + 4.8)$$

A similar procedure involving the oxidation peak was used to calculate the HOMO value. Oxidation and reduction potentials are given in Table ESI1.

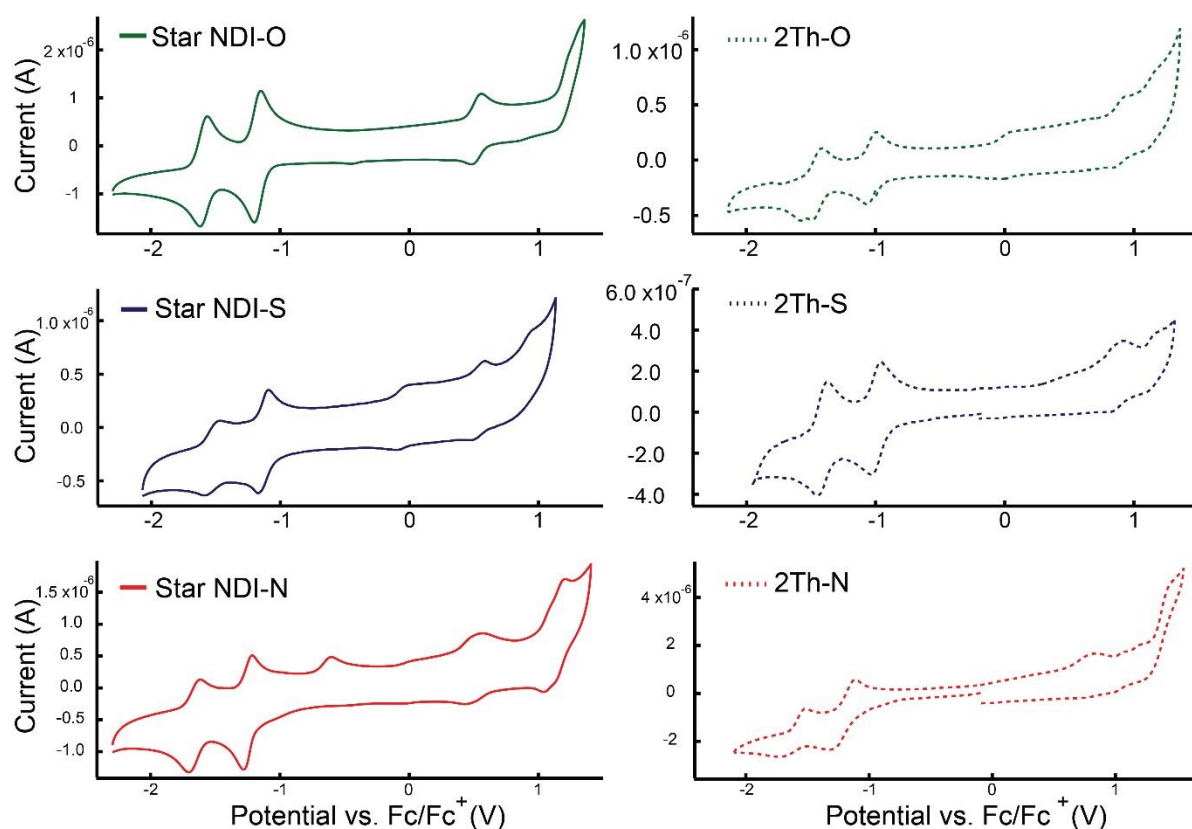


Figure ES20. Cyclic voltammograms for all six molecular acceptors.

Table ES1. Half-peak reduction and oxidation potentials as well as solution absorption onset values for each molecular acceptor.

Material	$E_{1/2}^{\text{FC/FC}^+}$ (V)	$E_{1/2}^{\text{red}}$ (V)	$E_{1/2}^{\text{ox}}$ (V)	$\lambda_{\text{abs, onset}}$ (nm)
Star NDI-O	0.26	-1.14	0.60	676
Star NDI-S	0.17	-1.13	0.52	709
Star NDI-N	0.09	-1.23	0.56	665
2Th-O	0.14	-1.03	0.88	648
2Th-S	0.19	-1.00	0.90	659
2Th-N	0.10	-1.21	0.71	647

A 0.1 g/l solution of each acceptor in chlorobenzene was used for all solution-based UV-Vis measurements. The solution absorption-onset wavelength was used to calculate the optical band gap in order to draw comparisons between the optical and electrochemically-based computed band gaps.

4. Absorbance

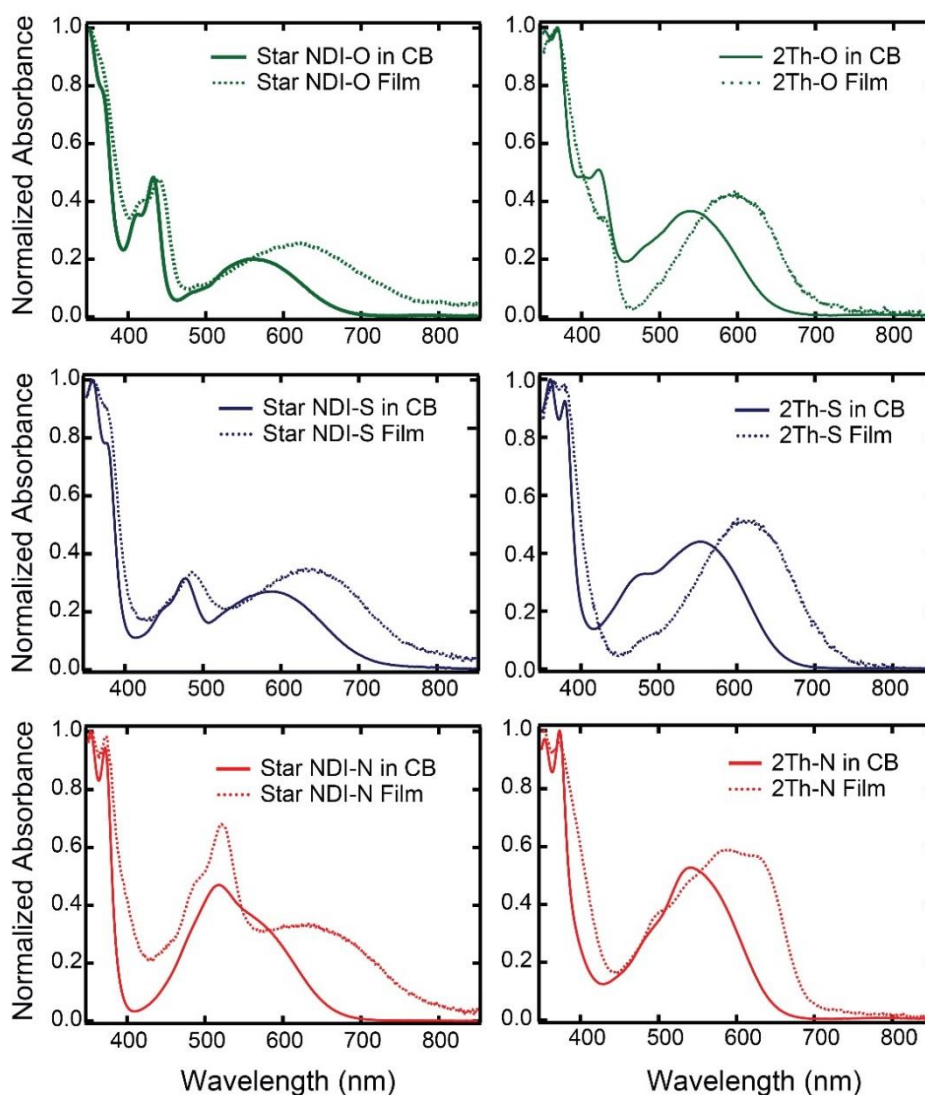


Figure ES21. Normalized solution and thin-film absorbance spectra for the acceptors.

A quartz vial was used for all solution and fused silica substrates with minimal reflectance were used for all solid-state UV-visible absorption measurements. These were both cleaned sequentially via sonication in acetone and 2-propanol for ten minutes. The molecules in solution were measured with a concentration of 0.1 g/l in chlorobenzene while films were spin cast at 6000 RPM from a 30 g/l solution in chlorobenzene. A Perkin Elmer Lambda 950 UV-Vis spectrometer was used for all measurements which were taken in the range from 350 nm to 900 nm. All films were normalized to the largest absorption peak, near or above 350 nm.

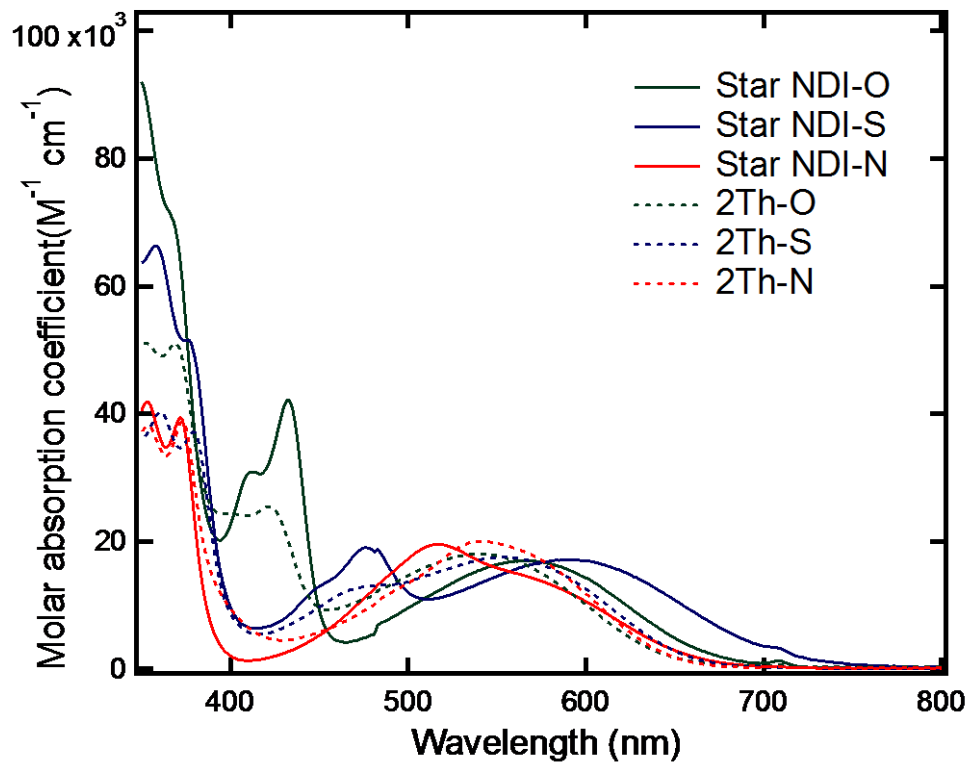


Figure ES22. Absorption spectra for all six molecular acceptors at room temperature in chlorobenzene.

5. Device Optimization

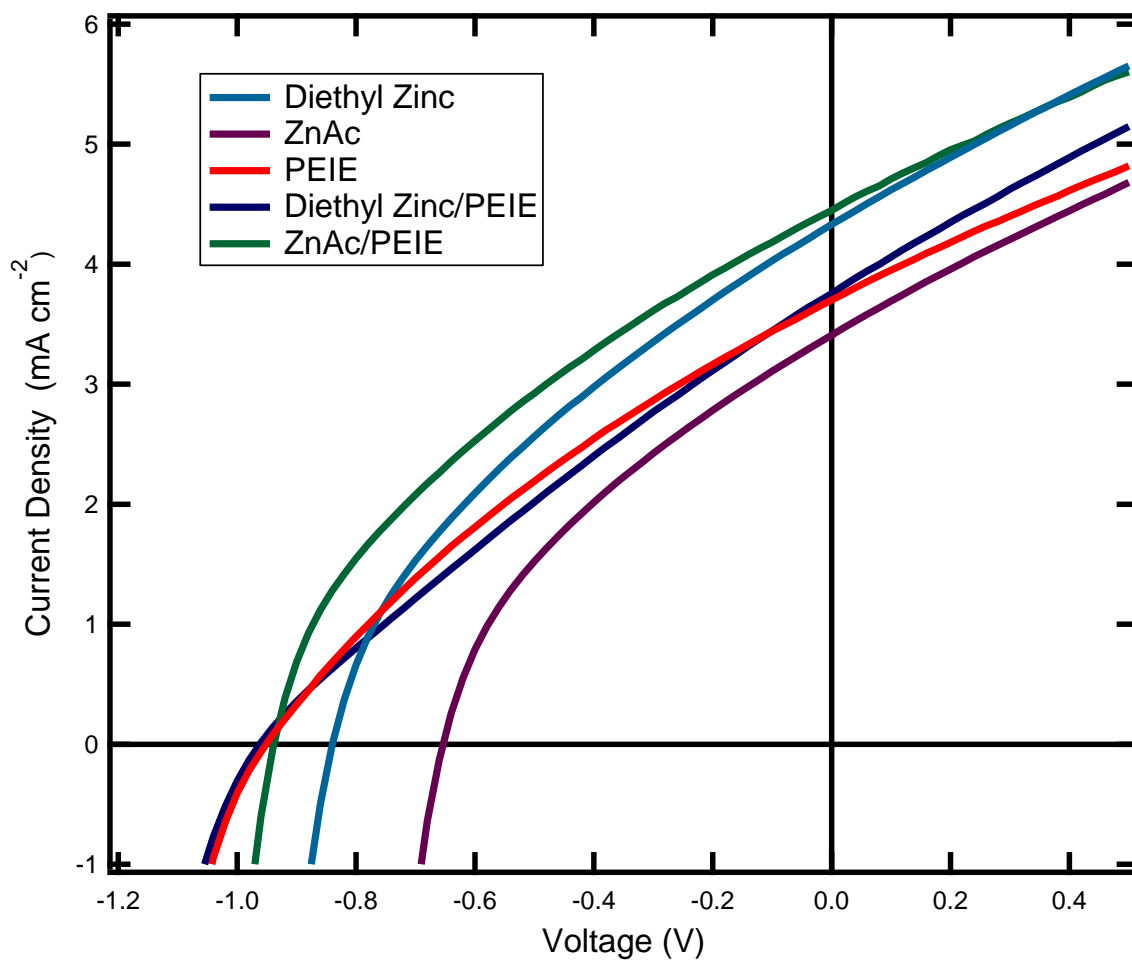


Figure ES23. J-V curves showing the electron transport layer comparison for devices made with Star NDI-O. Two different zinc oxide precursors were chosen: diethyl zinc solution (1:3 volume ratio in tetrahydrofuran) and zinc acetate. The double layer of ZnAc and PEIE was shown to increase the V_{OC} and J_{SC} over devices without the PEIE layer.

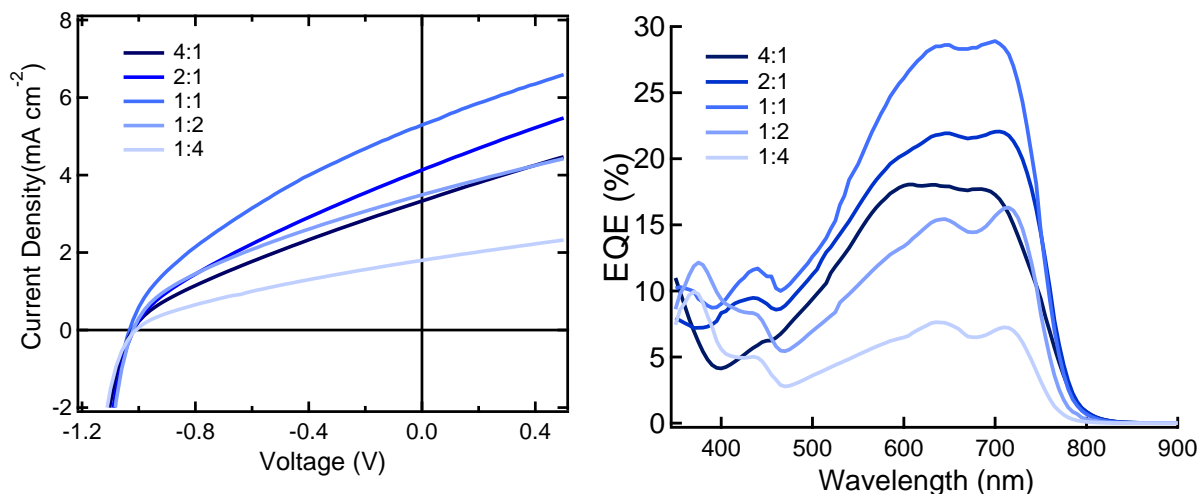


Figure ES24. J-V curves (left) and EQE spectra (right) of various donor:acceptor wt. ratios for PBDTTT-EFT:Star NDI-O devices. The optimal device performance was achieved at a 1:1 wt. ratio. Additional optimization includes experimentation with adding DIO as a solvent additive and film thickness.

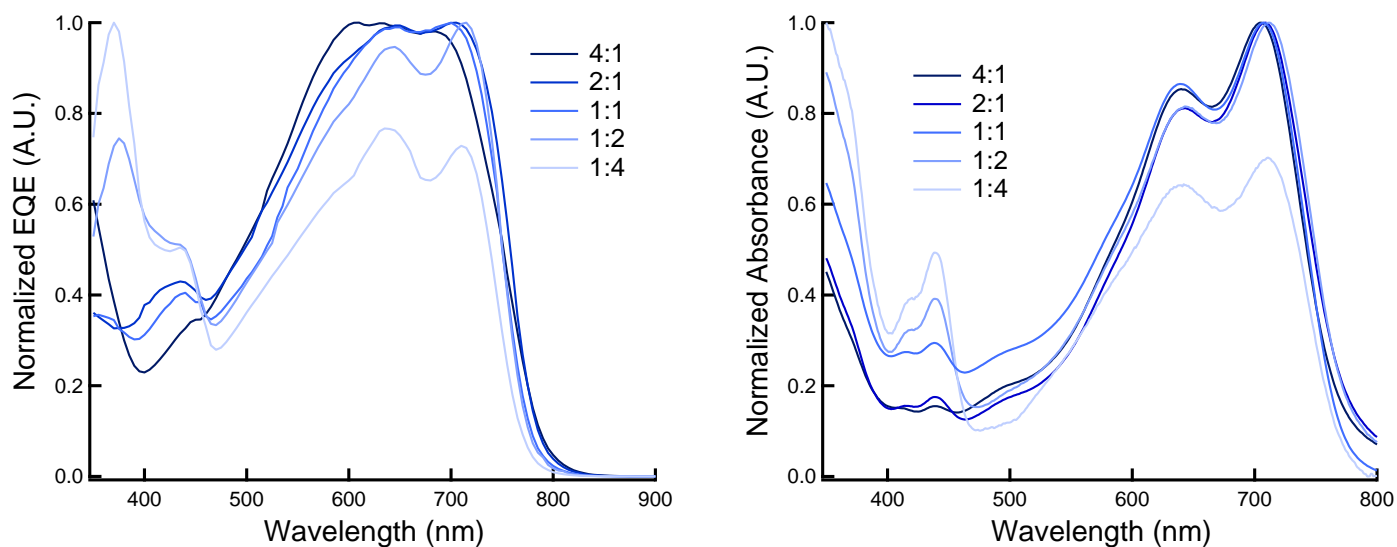


Figure ES25. Normalized EQE and Absorbance spectra for various donor:acceptor wt. ratios for PBDTTT-EFT:Star NDI-O devices. Analysis shows the donor material only modestly contributes to the devices' observed photocurrent.

Table ES1. *J-V* characteristics for Star NDI-O during optimization. Similar optimization was carried out for the other acceptors, and it was found the same processing conditions were optimal for each acceptor with PBDTTT-EFT.

Solvent	D:A ratio	% DIO	Spin Speed (RPM)	J_{sc} (mA cm⁻²)	V_{oc} (V)	FF (%)	PCE (%)
CB	4:1	0	6000	2.75	1.01	30.1	0.84
CB	2:1	0	6000	4.12	1.02	31.7	1.34
CB	1:2	0	6000	3.49	1.02	35.4	1.26
CB	1:4	0	6000	1.80	1.01	33.3	0.60
DCB	2:1	0	6000	4.16	0.93	37.0	1.43
DCB	1:1	0	6000	3.78	0.99	37.8	1.41
DCB	1:2	0	6000	1.56	0.80	36.0	0.45
DCB	1:1	0.5	6000	2.91	0.78	37.3	0.85
DCB	1:1	1.0	6000	2.85	0.96	33.3	0.91
CB	1:1	0	3000	4.79	1.00	35.6	1.71
CB	1:1	0.2	6000	4.70	1.01	34.5	1.63
CB	1:1	0.5	6000	4.41	0.98	33.3	1.45

6. 1D GIWAXS Line Cut Profiles

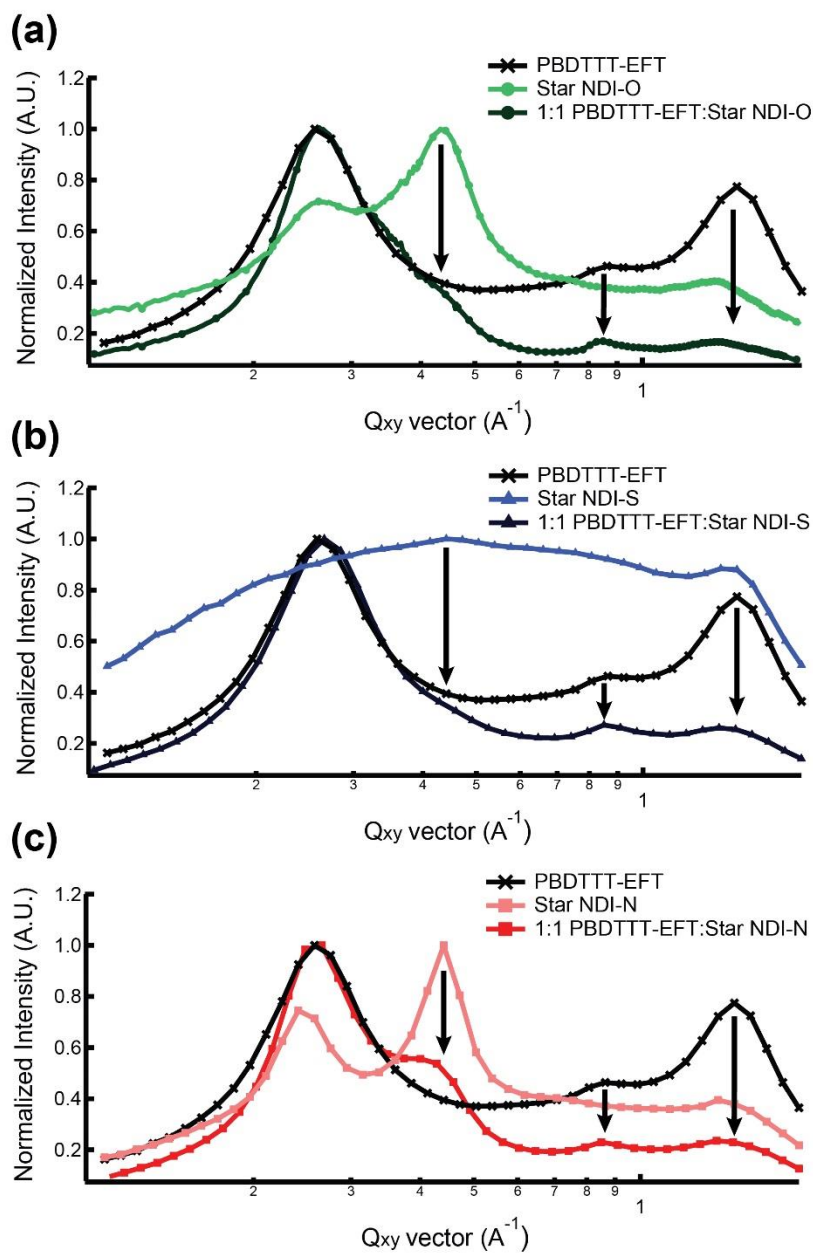


Figure ES26. Normalized 1D GIWAXS line cut profiles show the GIWAXS patterns for the blend films are a linear combination of the donor and acceptor materials, with the donor material largely dominating the film's overall crystallinity. Neat and blend line cuts for PBDTTT-EFT with Star NDI-O (a), Star NDI-S (b) and Star NDI-N (c) are shown.

7. Photoluminescence Quenching

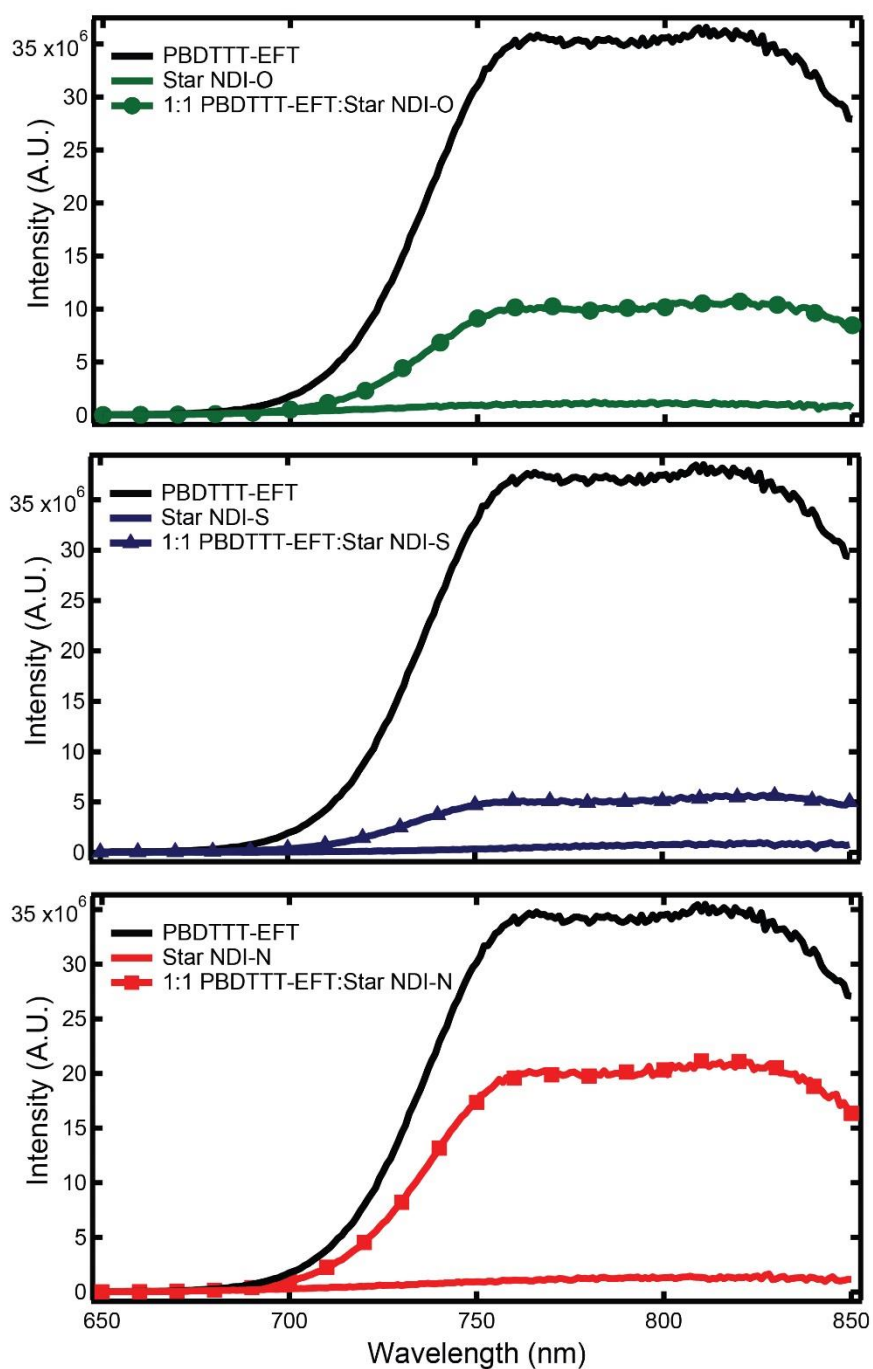


Figure ES27. Steady-state photoluminescence spectra for the three neat Star acceptors and neat PBDTTT-EFT as well as 1:1 blend films, which indicate varying PL quenching efficiencies. Excitation was at 600 nm and the photoluminescence intensity has been corrected.

8. SCLC Mobility for Star NDI-O

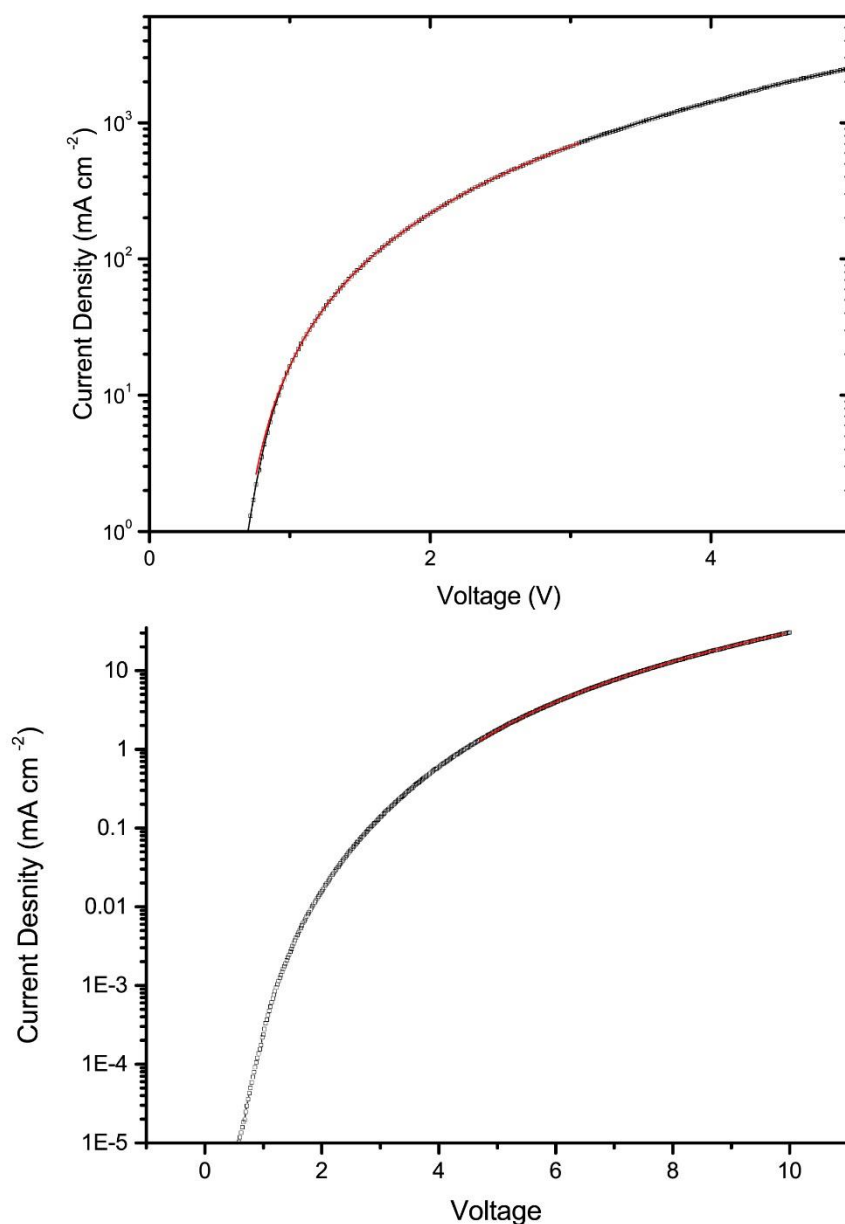


Figure ES28. J-V curves for SCLC devices made PBDTTT-EFT:Star NDI-O devices. Hole-only devices (top) were composed as follows: ITO/MoOx/Active Layer/Ag. Electron-only devices (bottom) had an ITO/ZnO/Active Layer/Ca/Al configuration. Mobility values of 4.6×10^{-4} cm² Vs for holes and 1.7×10^{-7} cm² Vs for electrons were computed.